Title	Development of an acetylacetonate-modified silica-zirconia composite membrane applicable to gas separation
Author(s)	Lawal, Sulaiman; Kanezashi, Masakoto; Nagasawa, Hiroki; Tsuru, Toshinori
Citation	Journal of Membrane Science , 599 : 117844
Issue Date	2020-04-01
DOI	10.1016/j.memsci.2020.117844
Self DOI	
URL	https://ir.lib.hiroshima-u.ac.jp/00050509
Right	© 2020. This manuscript version is made available under the CC-BY-NC-ND 4.0 license http://creativecommons.org/licenses/by-nc-nd/4.0/ This is not the published version. Please cite only the published version. この論文は出版社版ではありません。引用の際には出版社版をご確認、ご利用ください。
Relation	

Development of an acetylacetonate-modified silica-zirconia composite membrane applicable to gas separation

Sulaiman Lawal, Masakoto Kanezashi,* Hiroki Nagasawa, and Toshinori Tsuru

Department of Chemical Engineering, Graduate School of Engineering, Hiroshima University, 1-4-1 Kagamiyama, Higashi-Hiroshima 739-8527, Japan

*Corresponding author: E-mail address: kanezashi@hiroshima-u.ac.jp (M. Kanezashi)

Abstract

In this work, an acetylacetonate-modified equimolar SiO_2-ZrO_2 composite-derived membrane with molecular sieving properties was successfully fabricated. The sol-gel method was successfully employed to chemically modify zirconium tetrabutoxide prior to co-hydrolysis and -condensation with tetraethoxysilane, and it was then used to fabricate a gas separation layer. An acetylacetonate-modified SiO_2-ZrO_2-derived membrane prepared at 300 ºC showed H_2 permeance of 9.9×10^{-7} mol m^{-2} s^{-1} Pa^{-1} with a H_2/SF_6 permeance ratio of 7,600, which was a significant improvement over pure SiO_2-ZrO_2-derived membranes (H_2 permeance: 1.4×10^{-6} mol m^{-2} s^{-1} Pa^{-1}, H_2/SF_6 permeance ratio: 11). Heat-treatment of an $acac^-$-modified SiO_2-ZrO_2-derived membrane prepared at temperatures that ranged from 250 ºC (H_2 permeance: 4.5×10^{-8} mol m^{-2} s^{-1} Pa^{-1}, H_2/CH_4: 100, CO_2/CH_4: 60, H_2/SF_6: > 18,000 at 50 ºC) to 550 ºC resulted in an improved H_2 permeance of 3.4×10^{-6} mol m^{-2} s^{-1} Pa^{-1} with reduced permeance ratios (H_2/CH_4: 3, H_2/SF_6: 9) at 50 ºC. A membrane prepared by heat-treating a 250 ºC-fired membrane at 300 ºC showed the best trade-off with H_2 permeance-H_2/SF_6 permeance ratios above the trade-off line compared with membranes prepared at other temperatures.

Keywords: Silica-Zirconia; Acetylacetone; Chelating ligand; Chemical modification; Gas separation

1. Introduction

The quest for a highly efficient and cost-effective means for separating important gases and liquids has gained prominence in the field of separation technology in the past century. Such research efforts have successfully yielded a variety of techniques such as membrane separation technology, which has attracted the most interest [1]. Inorganic membranes are currently in great demand for use in H_2 [2-5, 6], CO_2/CH_4 [7, 8], and CO_2/N_2 [9, 10] separation systems, as well as in olefin/paraffin systems [11, 12] and in the purification of natural gas [11]. Inorganic membranes can be broadly divided into porous and dense versions. Whereas dense membranes such as those fabricated from palladium and its alloys offer separation ability via a solution-diffusion mechanism, porous inorganic membranes such as silica, alumina, and zirconia separate gases by selective passage of molecules through a network of pores according to their size. Palladium membranes have shown high H_2 permeance, but they are difficult to fabricate and are plagued by high module costs [13, 14]. A mixed-matrix membrane consisting of palladium or palladium-cobalt particles dispersed in a network of amorphous inorganic silica is also possible as already reported by Kanezashi *et al.* [15] and Ballinger *et al.* [16].

Much interest has been shown to inorganic amorphous silica membranes and their derivatives concerning their potential application to a wide variety of gas separation systems in general [2-11], and in particular to hydrogen separation due to their ease of fabrication, low cost of production and scalability [1]. Factors required for a perm-selective membrane are high flux, high selectivity, pore size controllability, and good physical and chemical stability. Silica membranes exhibit moderately high flux and excellent selectivity [15, 17, 18], but size control and instability under hydrothermal conditions are known problems [15]. To develop silica and silica-based membranes with high perm-selectivity, pore size tunability, and hydrothermal stability, many researchers have studied various techniques such as spacer methods [19, 20], templating methods [21], anion and cation doping [6, 17, 23], and hybridization of silica with other metal oxides such as Al_2O_3 [12, 24], TiO_2 [25, 26], and ZrO_2 [5, 22].

Hybridization of silica with proven hydrothermally stable metal oxides such as TiO_2 and ZrO_2 has been studied extensively [1, 5, 22, 26, 27]. Hybrid SiO_2-ZrO_2 membranes have been used for pervaporation and nanofiltration applications [27, 28]. Hydrogen separation performance of SiO_2-ZrO_2 hybrid membranes fabricated through chemical vapor deposition (CVD) has also been investigated [5]. Zirconium oxide added to silica in an equi-molar ratio has shown the best hydrothermal stability to moderately high temperatures, but perm-selectivity remains very poor due to the large pore size created by adding a high zirconia content [22]. The large pores permit both large and small molecules to permeate as in Knudsen flow [29, 30]. However, a further modification to this network structure offers the possibility to change the molecular sieving characteristics of silica-zirconia (1:1) composite membranes.

In the fields of catalysis and separation technology, the versatility of sol-gel chemistry has been instrumental to the formation of new functional materials. One major aspect of this versatility is the ability to obtain products with predetermined characteristics based on the experimental conditions, and another aspect is that it allows for the synthesis of inorganic-organic hybrid materials through the introduction of organic groups in solution [31]. One way to add an organic group is to chemically modify a precursor prior to synthesis [32]. A good example of chemically modifying precursors is found in the use of chelating ligands to form coordinate complexes where the precursor to be modified is a transition metal ion compound. Coordinate polymer chemistry has been widely studied and found to be useful in synthesizing metal-organic frameworks (MOFs) [33-35]. Coordinate covalent bonds are formed in coordinate complexes by the occupation of d-orbitals belonging to a transition metal by free electron pairs donated by chelating ligands. For polydentate ligands, Metal-Organic Frameworks (MOFs) usually result [33-35]. In the case of mono- or bidentate ligands, MOFs are rarely formed [36, 37] and the formation of the coordinate complex chains will require other polymerization sites.

The formation of coordination complexes between zirconium ions and various chelating ligands has been studied [36, 38] with the most hydrolytically stable being the use of acetylacetone (Hacac), a bidentate ligand, to form an acetylacetonate-zirconium coordination complex [38], which implies the retention of acetylacetonate anions in the polymer sol even after hydrolysis and condensation have occurred for several hours. As such, a hydrolytically stable modified zirconium precursor can be co-polymerized and co-condensed with silica to achieve an $acac^-$-modified equi-molar SiO_2-ZrO_2 polymer sol. The acetylacetone ligand remaining in the modified SiO_2-ZrO_2 (1:1) is expected to translate into a modified pore structure applicable to gas separation. This possibility has been reported by both Fukumoto *et al.* [39] and Spijksma *et al.* [40], where the pore sizes of TiO_2-ZrO_2 were controlled using isoeugenol (isoH) and diethanolamine (DEA), respectively.

To study the possibility of a chemically modified silica-zirconia (1:1) membrane for gas separation applications, acetylacetone-modified silica-zirconia (1:1) was prepared by the sol-gel method and used to fabricate a membrane. Single-gas permeation measurements were subsequently performed. Fig. 1 schematically shows the theoretical modification of zirconium tetra butoxide with acetylacetonate and the subsequent formation of an $acac^-$-modified Si-O-Zr network. Theoretically, acetylacetone is a bidentate ligand with two sites through which it can bond to transition metal zirconium ions in order to form a normal covalent bond with zirconium through one of the oxygen atoms and a coordinate covalent bond by donating a free pair of electrons from the other oxygen atoms that occupy the empty d-orbital. This theory assumes that acetylacetone approaches the zirconium ions in its enol tautomer [36]. Furthermore, the thermal stability of the acetylacetonate modifying ligand was examined, and the pore modification effect that the addition of acetylacetonate ligands and heat-treatment exerted on the pore structure and on the gas permeation characteristics were explored. Activation energies were used to compare the SiO_2-ZrO_2-$acac_2$ (SZa_2) membrane performance with that of both a polymer membrane and a ligand-modified TiO_2-ZrO_2 membrane.

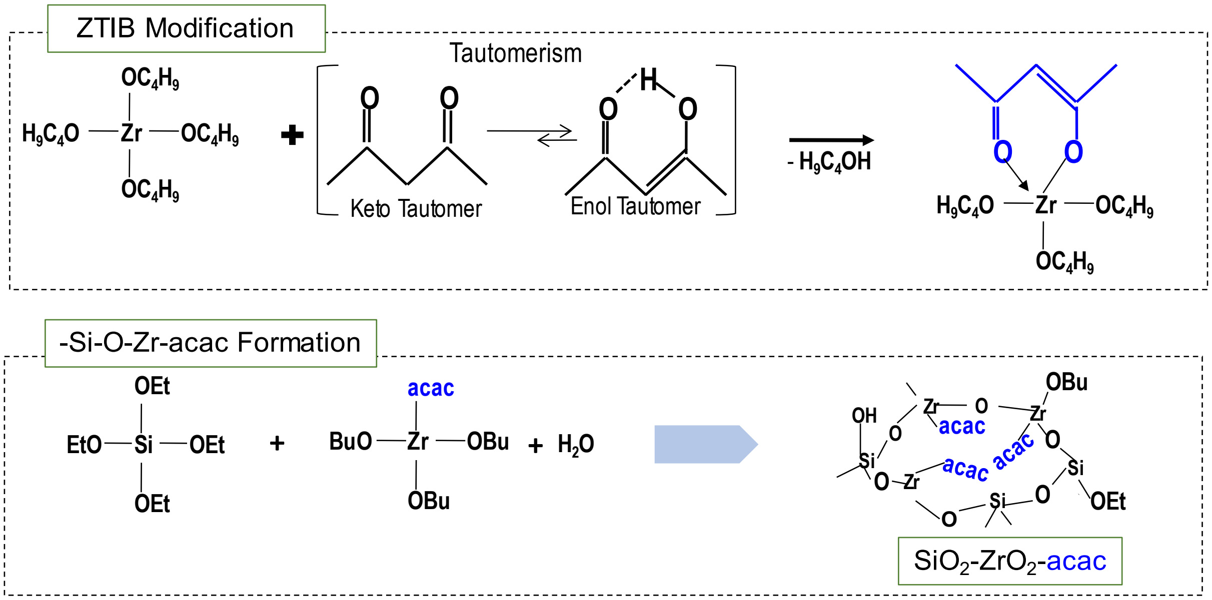

Fig. 1 Theoretical formation of the -Si-O-Zr-acac linkages in a polymer sol

2. Experimental

2.1 Preparation of SiO_2-ZrO_2-acac$_2$ sol and membrane fabrication

A 5 wt% modified SiO_2-ZrO_2 (1:1) polymeric sol (referred to as SZa$_2$ sol in later sections) and membranes were prepared and fabricated according to the following procedures. Modified SiO_2-ZrO_2 (1:1) sol was prepared in two stages. In the first stage, an 80% pure zirconium (iv) tert-butoxide (Aldrich) dissolved in ethanol (Aldrich) was modified by reacting with 99% pure acetylacetone (Aldrich) (ligand/ZrTB molar ratio 2) for one hour in the proportions listed in Table S1. In the second stage, a solution of 98% pure tetraethoxysilane (Aldrich) in ethanol was co-hydrolyzed with acetylacetone-modified zirconium (iv) tert-butoxide in a molar ratio of 1:1 using deionized water (water/ZrTB molar ratio 4) and hydrochloric acid (37%, Nacalai Tesque) as a catalyst (acid/alkoxide molar ratio 0.25). Hydrolysis and poly-condensation were carried out by stirring the mixture at 500 rpm for more than 12 hours at room temperature.

In a similar manner, without pre-modification of zirconium (iv) tert-butoxide, a 5 wt% unmodified SiO_2-ZrO_2 (1:1) polymeric sol (referred to as SZ sol in later sections) was prepared in a process that required only one stage. The size of the resultant SiO_2-ZrO_2-$acac_2$ sol, as measured by Dynamic Light Scattering (Malvern), is presented in Figure S1. The chemical reagents and their respective proportions are also summarized in Table S1. Dried gels were prepared by drying the sols slowly at a temperature of about 50 °C for a few days.

SiO_2-ZrO_2-$acac_2$ membranes were fabricated by coating 3 graded layers of different suspensions/sols onto cylindrical α-alumina porous supports (60% porosity; 1.2 µm pore size; outer diameter, 1 cm; and, length, 10 cm; Nikkato Corporation, Japan) connected to non-porous supports that were closed and open at either end. The first layer was prepared by coating a 10 wt% suspension of α-alumina particles (diameter 2-3 µm and 0.2 µm) onto a colloidal SiO_2-ZrO_2 sol for use as a binder prepared by ultrasonification. The preparation of colloidal SiO_2-ZrO_2 sol has been described elsewhere [28]. Each coating was repeated 6 times, and each coating was fired to a temperature of 550 °C for 15 – 20 min to solidify and bind the particle layer to the support and to cover the larger pores of the porous alumina support.

Next, pure SiO_2-ZrO_2 (1:1) sol diluted to 0.5 wt% with deionized water was coated onto the α-alumina particle layers using a hot coating method to form an intermediate layer, where the membrane was pre-heated to about 200 °C, and then coated almost immediately with the SiO_2-ZrO_2 sol followed by firing at 550 °C for 15 – 20 min to bind the intermediate layer to the particle layer. This process was repeated several times until large pores and defects from the particle layer were covered and a narrow pore size distribution suitable for the separation layer coating was achieved. The pore size distribution was obtained by nanopermporometry [41]. The top separation layer was comprised of the acetylacetonate-modified SiO_2-ZrO_2 (1:1) polymeric sol (derived from diluting the as-prepared sol to 0.5 wt% in ethanol) coated onto the SiO_2-ZrO_2 intermediate layer followed by firing under a 600 ml min^{-1} nitrogen gas flow at 250 °C for 15 min in a tube furnace. After this process was repeated 6 – 8 times, the membrane fabrication process was concluded, and the membranes were ready for single-gas permeation measurements. The same procedure was followed for the fabrication of an unmodified SiO_2-ZrO_2 (1:1) membrane that was used for comparison.

2.2 Characterizations of the SiO_2-ZrO_2-acac$_2$, the SiO_2-ZrO_2 sol, the gel, and the membranes

The particle sizes of the as-prepared sols were analyzed at 25 ºC via dynamic light scattering (DLS) using a Malvern Zetasizer Nano ZS (Malvern Instruments Ltd.). The presence and intensities of different functional groups were analyzed via Attenuated Total Reflection-Fourier Transform Infrared Spectroscopy (ATR-FTIR, FTIR-4100, JASCO, Japan). This analytical method was also used to track the thermal stability of ligands. Thermal stability of the acetylacetonate ligands in modified SiO_2-ZrO_2 was analyzed using thermogravimetry (TG, TG-50 Shimadzu Co., Japan) under a nitrogen gas flow of 80 ml min^{-1} and a heating rate of 10 ºC min^{-1}. The cross-section and surface morphologies were examined by Field Emission-Scanning Electron Microscopy (FE-SEM, Hitachi S-4800, Japan). Prior to examination, shared samples of the membranes were attached to sample holders via carbon tape and vacuum-dried at 50 ºC for 48 hours.

2.3 Single-gas permeation measurements

A schematic representation of the gas permeation measurement setup is shown in Fig. 2. Prior to the gas permeation measurement, a membrane was fitted into its module immediately after fabrication and placed inside the furnace in the gas permeation measurement rig at a temperature of 150 or 200 ºC under helium flow of 100 ml min^{-1} for about 12 hours. This was done to ensure the removal of water adsorbed into the membrane pores after fabrication. To test for the molecular sieving properties of the membranes, high-purity gases (H_2, He, CO_2, N_2, CH_4, CF_4, SF_6 in that order) were flowed through molecular sieves to remove humidity, and were then fed to the feed side of the membrane module at 100 kPa gauge pressure at temperatures ranging from 50 – 200 ºC. Permeate side pressure was kept atmospheric and permeate gas flow was measured using a bubble film flow meter (HORIBA-STEC, Japan). Temperature dependence of gas permeance was examined by varying the temperature during the flow of a single gas and measuring the permeance flow at each desired temperature. It should also be noted that permeate gas flow was only recorded after a steady state was attained.

Membrane heat-treatment was done by heating the membrane fired at 250 °C in the membrane module to a higher temperature (300, 400 or 550 °C) while flowing N_2 gas through the membrane. The flow of N_2 was maintained until a steady state was reached and the single-gas permeance was subsequently measured at 200 °C. This procedure was repeated for each heat-treatment temperature.

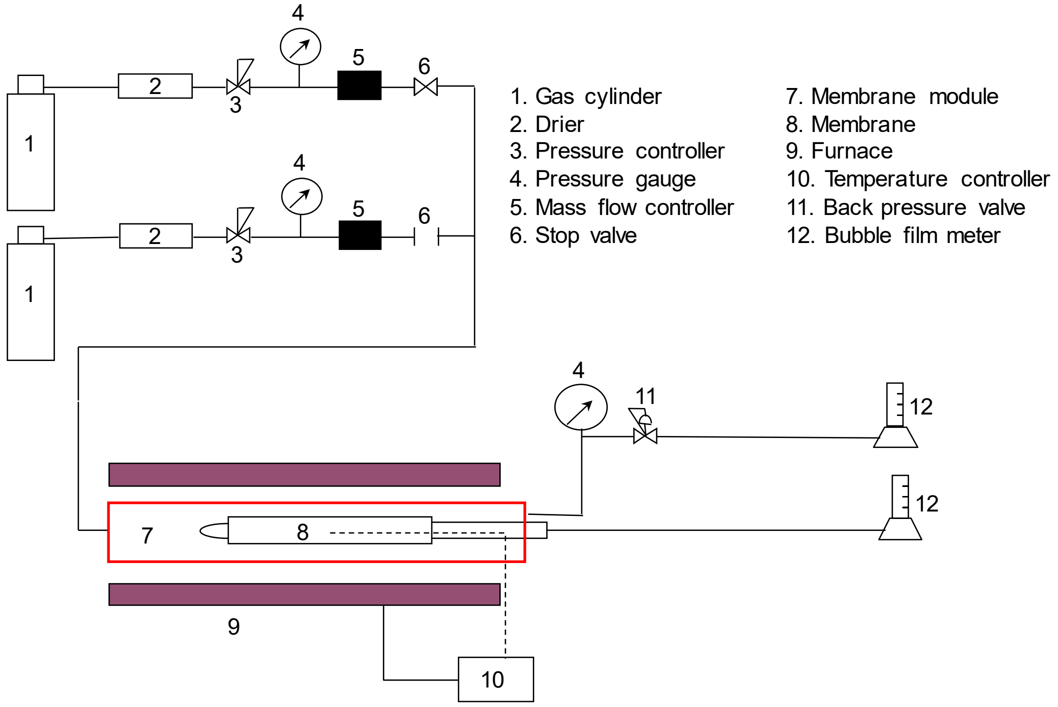

Fig. 2 Schematic diagram of single-gas permeation measurement**.**

3. Results and Discussion

3.1 Sol-gel characterization

3.1.1 Chemical modification of a ZrTB precursor

Fig. 3 shows the ATR-FTIR spectra of freshly prepared modified and pure zirconium tetrabutoxide precursors, measured directly on an ATR prism window that ranged from 4,000 to 500 cm^{-1} compared with that of acetylacetone (Hacac). Peaks ranging from 1,700 to 1,500 cm^{-1} are magnified for clarity in Fig. 3 (b). The two peaks that appear around 1,600 cm^{-1} and 1,525 cm^{-1} were assigned to the enol C=O and C=C bonds that are characteristic of the acetone species [36, 38]. The presence of the C=C bond supports the assumption that Hacac approaches ZrTB in its enol tautomer. These peaks were not detected for the unmodified precursor and Hacac, which presented only the C=O (1615 cm^{-1}) peak of the keto tautomer. This clearly indicates the introduction of the acetylacetonate group to the chemical structure of zirconium tetrabutoxide. Furthermore, peaks assigned to the butoxide groups ($-CH_2$, $-CH_3$) in the range of 3,000 to 2,750 cm^{-1} were observed for both modified and pure zirconium tetrabutoxide precursors, although different peak heights were exhibited. The $-CH_2$, $-CH_3$ peaks observed for the modified zirconium tetrabutoxide precursor were shorter than those observed for the unmodified precursor with representative absorbance peak ratios, A_{2960}/A_{1400}, of 0.29 and 0.56 for modified ZrTB and pure ZrTB, respectively. A_{2960} represents the absorbance peak height of a $-CH_2$ bond normalized by a common Zr-O-C peak observed at around A_{1400} (1,400 cm^{-1}). This indicates the replacement of some butoxy groups by the acetylacetonate groups that would have been otherwise present without modification.

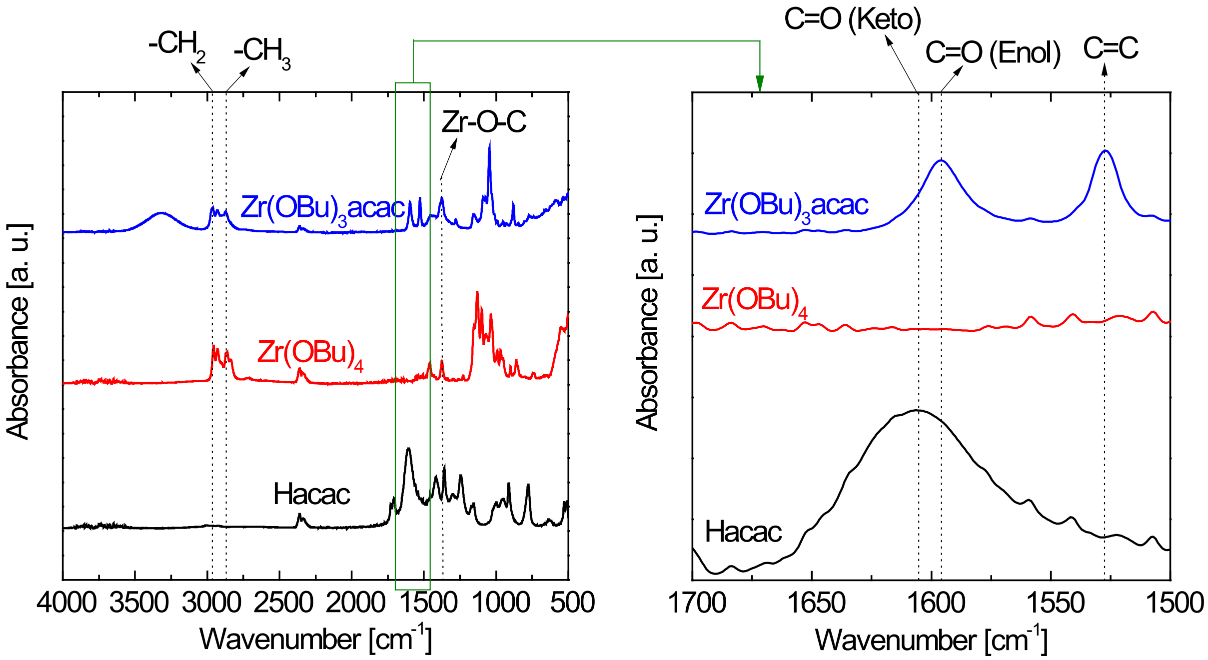

(a) (b)

Fig. 3 ATR FT-IR spectra of ZrTB (zirconium tetrabutoxide) modification by acetylacetonate ligands ranging (a) from 4,000 to 500 cm^{-1} and (b) from 1,700 to 1,500 cm^{-1}.

Fig. 4 also shows highly magnified ATR-FTIR spectra ranging from 1,700 to 1500 cm^{-1} that compare modified zirconium tetrabutoxide, modified silica-zirconia, and pure unmodified silica-zirconia sols. The C=O and C=C peaks characteristic of acetylacetonate ligands observed for the modified zirconium tetrabutoxide precursor were also detected for the modified silica-zirconia sol. This is an indication that the acetylacetonate-zirconium chelation structure was unaffected by the introduction of silica. Furthermore, the acetylacetonate characteristic peaks (1,600 cm^{-1} and 1,525 cm^{-1}) in the modified silica-zirconia sol were absent from the unmodified sol, which suggests that acac$^-$ ligands are hydrolytically stable, and were not hydrolyzed by the addition of water under acidic conditions. This was previously observed during hydrolyzation of the acac-ZrTB coordinate complex polymer for several days [36]. The rate of ZrTB hydrolysis is much faster than that of TEOS, and one advantage of modifying the zirconium tetrabutoxide with a hydrolytically stable ligand prior to mixing with TEOS was that the hydrolysis rate of ZrTB was slowed considerably so that during co-hydrolysis of the ZrTB and TEOS mixtures, the rates of hydrolysis were similar, which improved the -Si-O-Zr- composition degree [32].

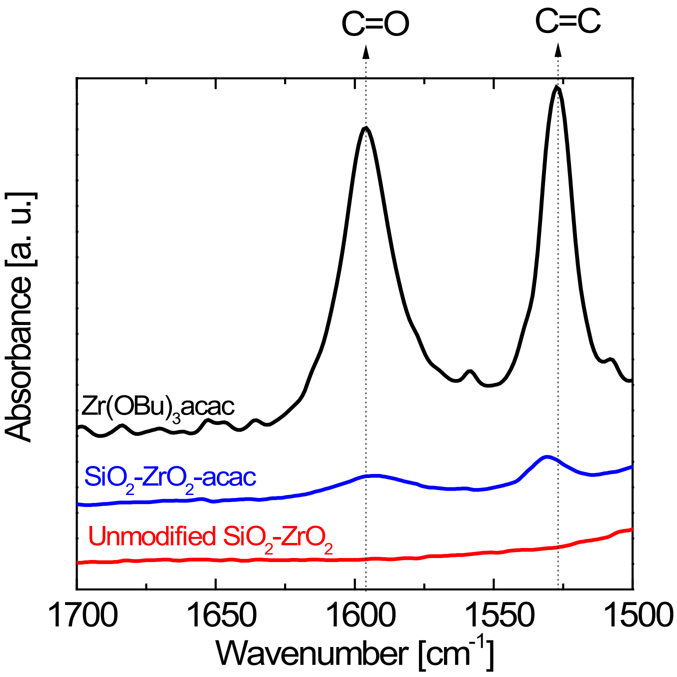

Fig. 4 ATR-FTIR spectra ranging from 1,700 to 1,500 cm^{-1} for modified zirconium tetrabutoxide, modified silica-zirconia, and unmodified silica-zirconia sols.

3.1.2 Thermal analysis of acac$^-$ ligands in SiO_2-ZrO_2-acac$_2$ gels

The hydrolytic stability of acac in the sol phase was expected, having been established in section 3.1.1, and this section discusses the thermal stability of the acac$^-$ ligands in the SZa$_2$ powder. The thermogravimetric (TG) curves of pure SiO_2-ZrO_2 and SiO_2-ZrO_2-acac$_2$ gels fired under a N_2 flow at temperatures as high as 1,000 °C (ramping rate: 10 °C min^{-1}) and the ATR-FTIR spectra of SZa$_2$ powders fired under N_2 at different temperatures are shown in Fig. 5. In Fig. 5(a), the TG profile of SZa$_2$ powder can be divided into 3 sections according to their different slopes. Section i (100-300 °C) can be assigned to the decomposition of unhydrolyzed butoxy groups and to the partial decomposition of acetylacetonate linkages based on weight loss. This is supported by the ATR-FTIR profile of powders fired at different temperatures (Fig. 5(b)).

In section ii (300 and 500 °C), pure SZ powder exhibited no further weight loss beyond 300 °C, indicating that weight loss was due only to the decomposition of unhydrolyzed butoxy groups. For SZa_2 powder, further weight loss was observed to a residual weight ratio that reached as high as 0.7, indicating the complete decomposition of acac ligands. This also appears in Fig. 5 (b) as the characteristic C=O and C=C bonds were decreased with temperature. Beyond 500 °C, as shown in section iii, free carbon from the decomposed acac$^-$ ligands was released into the pore network, which resulted in no observed weight loss in this region. The dark appearance of the residual powders after TG measurement supports the theory of the encapsulation of free carbon in the SiO_2-ZrO_2 network (see Fig. S2), which is similar to carbon-encapsulated nickel nanoparticles prepared by the instant pyrolysis of nickel acetylacetone reported by Chen *et al.* [42], as well as the C/C-ZrC composites fabricated by zirconium acetylacetone pyrolysis [43]. The continued weight loss of SZa_2 powder beyond 300 °C indicates that an acac$^-$-modified SiO_2-ZrO_2 layer can be fabricated even when fired to a temperature as high as 300 °C.

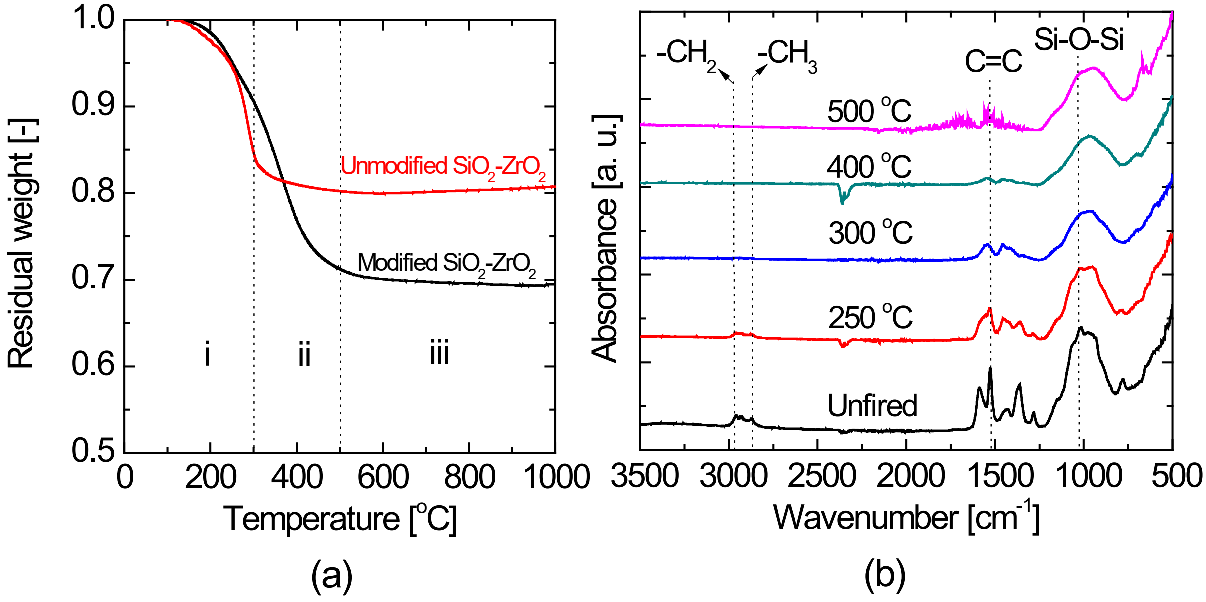

Fig. 5 TG curves of pure SiO_2-ZrO_2 and SiO_2-ZrO_2-$acac_2$ gels under N_2 at temperatures as high as 1,000 °C (a) and Powder ATR-FTIR spectra of SiO_2-ZrO_2-acac gels fired under a N_2 atmosphere at different temperatures (b)

Fig. 5 (b) shows the ATR-FT-IR spectra of SZa_2 powders fired under N_2 at different temperatures. The peak at around 1,500 cm^{-1} was assigned to the C=C bond characteristics of an acetylacetonate ligand, as mentioned in a previous section [36, 38]. The presence of this peak is indicative of the fact that the acac-Zr chelation structure was unaffected by the change of state from sol to gel. The peak stretching between 1,100 and 900 cm^{-1} was assigned to the -SiOSi- ring while the -SiOH group was assigned to the peak at about 800 cm^{-1}. The peaks between 2,800 and 3,000 cm^{-1} were assigned to the unhydrolyzed ethoxy and butoxy groups [44-46]. The -SiOSi- peaks were detected irrespective of the firing temperature, which is indicative of the formation of silica networks by hydrolysis and by the condensation of the ethoxy groups of TEOS. The C=C peaks began to disappear as the firing temperature increased and the relationship between the $A_{C=C}/A_{\text{-SiOSi-}}$ absorbance peak ratio and firing temperature appeared to be inversely linear, as shown in Fig. S3.

The simultaneous reduction and disappearance of $-CH_2$, $-CH_3$ and -SiOH peaks at temperatures higher than 300 °C was confirmed along with the subsequent -SiOSi- peak shift and broadening. This can be attributed to the condensation of ethoxy, butoxy and silanol groups and the formation of more -SiOZr- connections. The broadening and red shift of the -SiOSi- peak in a silica-zirconia composite FT-IR spectrum is indicative of more -SiOZr- connections, and the inclusion of Zr^{4+} ions into the -SiOSi- ring caused a ring deformation and a resultant peak shift and broadening [47]. Fig. S4 shows the XRD patterns of pure SZ-derived and SZa_2-derived powders after firing at 700 °C under N_2. After firing at 700 °C, the tetragonal ZrO_2 peaks at $2\theta = 30^{\circ}$ and 50° indicated that the pure SZ-derived powder had begun to show an aggregation of ZrO_2 crystallites, whereas SZa_2-derived powder remained amorphous without aggregation of ZrO_2 crystallites indicating a better -Si-O-Zr- composition degree.

3.2 Effect of acetylacetonate ligands on the pore size controllability of SiO_2-ZrO_2 (1:1) membranes

Fig. 6 shows the kinetic diameter dependence of single-gas permeance at 200 °C (a) and dimensionless permeance based on He (b) for SZ and SZa_2-derived membranes prepared at 300 °C under a N_2 atmosphere. Pure SZ-derived membranes showed a higher gas permeance compared with that of SZa_2-derived membranes, but He and H_2 selectivity over other gases was approximately the same as the Knudsen ratio. For example, a pure SZ-derived membrane showed a H_2 permeance of 1.4×10^{-6} mol m^{-2} s^{-1} Pa^{-1} with a H_2/SF_6 permeance ratio of 11.

The SZa_2-derived membrane showed a trend similar to that of the SZ-derived membrane; He (0.26 nm) permeance was lower than that of H_2 (0.289 nm), and N_2 (0.364 nm) permeance was lower than that of CH_4 (0.38 nm). This suggests a network pore size large enough for the separation of He-H_2 and N_2-CH_4 and Knudsen diffusion that is dominated by the permeation properties [29, 30]. However, the SZa_2-derived membrane showed a low SF_6 permeance of 1.3×10^{-10} mol m^{-2} s^{-1} Pa^{-1}, with a high H_2/SF_6 permeance ratio of 7,600. This shows that the chelation of Zr^{4+} with $acac^-$ ligands uniformly modified the pores of the SZa_2-derived membrane for molecular size-dependent permeation resistance. SZa_2-derived membranes, therefore, show promise for the separation of H_2/large organic gases, because the molecular size of SF_6 (0.55 nm) is similar to that of organic gases in benzene-cyclohexane and toluene-MCH systems (0.585 and 0.6 nm respectively) [48].

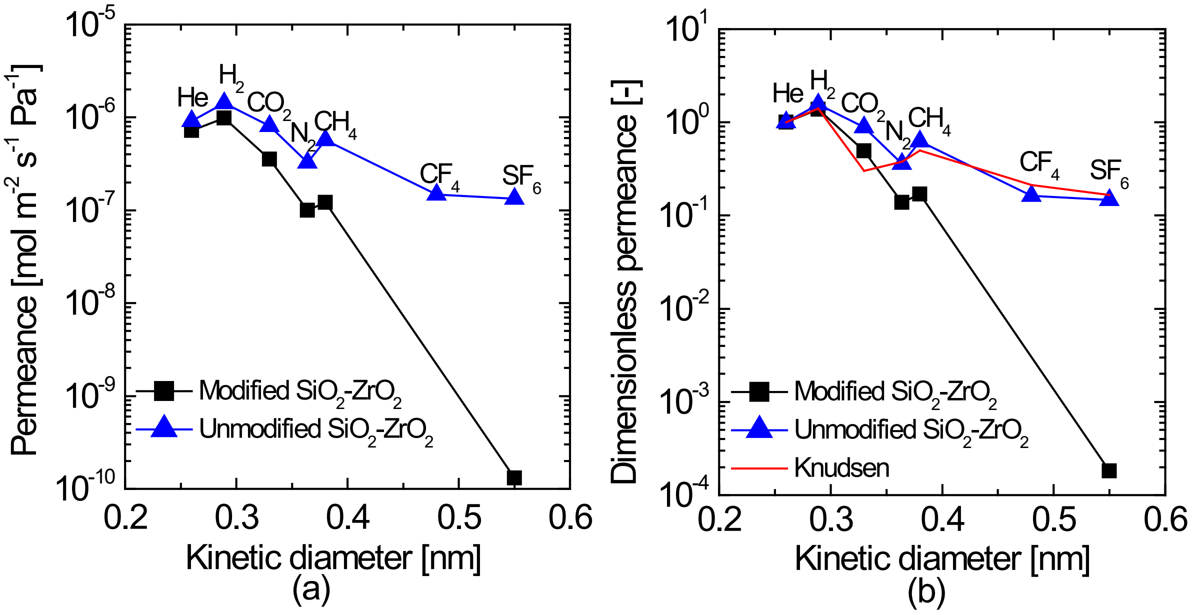

Fig. 6 Molecular size dependence of gas permeance (a) and dimensionless permeance based on He (b) at 200 °C of SiO_2-ZrO_2-acac$_2$ and pure SiO_2-ZrO_2 membranes all prepared at 300 °C under a N_2 atmosphere.

Fig. 7 shows the FE-SEM cross-sectional morphologies (x 50,000) of SZa$_2$ (a) and pure SZ (b)-derived membranes. A thin separation layer of acac$^-$ modified silica-zirconia was successfully fabricated, although it was indistinguishable from the intermediate layer at this magnification. The α-Al_2O_3 particle layer (average 1 μm) was clearly distinguishable as a compact impenetrable support for the intermediate and top layers (< 400 nm) of both membranes. It should be noted that the FE-SEM images were taken after gas permeation experiments were performed. The lamination of the SZ and SZa$_2$ that topped the SiO_2-ZrO_2 intermediate layers was retained after gas permeation experiments, which suggests a favorable interaction between silica-based top layers containing organic groups and the SiO_2-ZrO_2 layer. Therefore, the addition of the acac$^-$ ligands to SiO_2-ZrO_2 had no structural effect on the top layer during long-term use.

The schematic diagram in Fig. 8 (a) summarizes the effect of the acac$^-$ chelating ligands on the Si-O-Zr network. The chelation of acac$^-$ ligands to Zr$^+$ sites created network spaces small enough to prevent permeation by large gases yet large enough to allow small gases to permeate, which created better molecular sieving properties. Hypothetically, as Fig. 8 (b) illustrates, interlayer condensation may occur between two successive layers when the free chelation sites in $acac^-$ ligands on one layer chelate with the Zr^+ sites on another layer. Such interlayer interactions like the self-assembly of thiourea-crosslinked graphene oxide [49], topotactic dehydration-condensation of layered silicate into a zeolite [50], and hydrogen-covalent bond interaction between hybridized layers of PVA/TEOS [51] have been studied and proven. Characterization to prove these types of interaction is currently beyond the scope of this study and will require further inquiry. This phenomenon was not apparent in the SEM micrographs even at very high magnification.

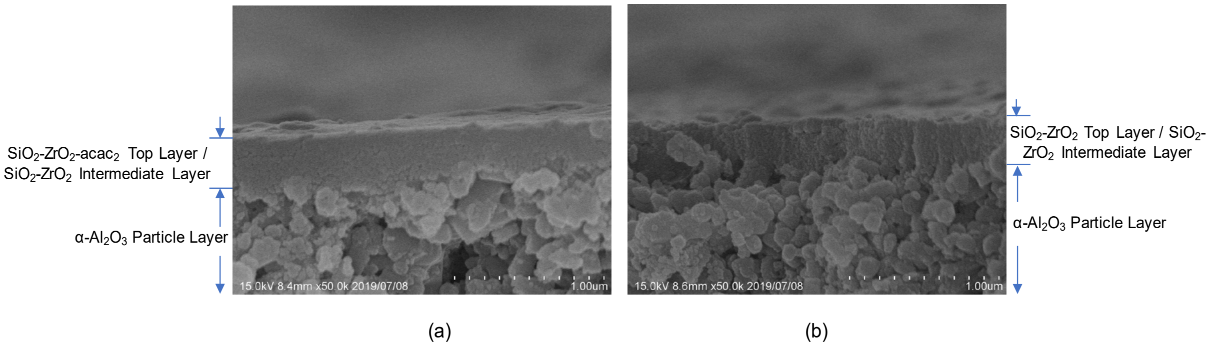

(a) (b)

Fig. 7 FE-SEM micrographs of the cross-section for SiO_2-ZrO_2-$acac_2$ (a) and pure SiO_2-ZrO_2 (b) membranes.

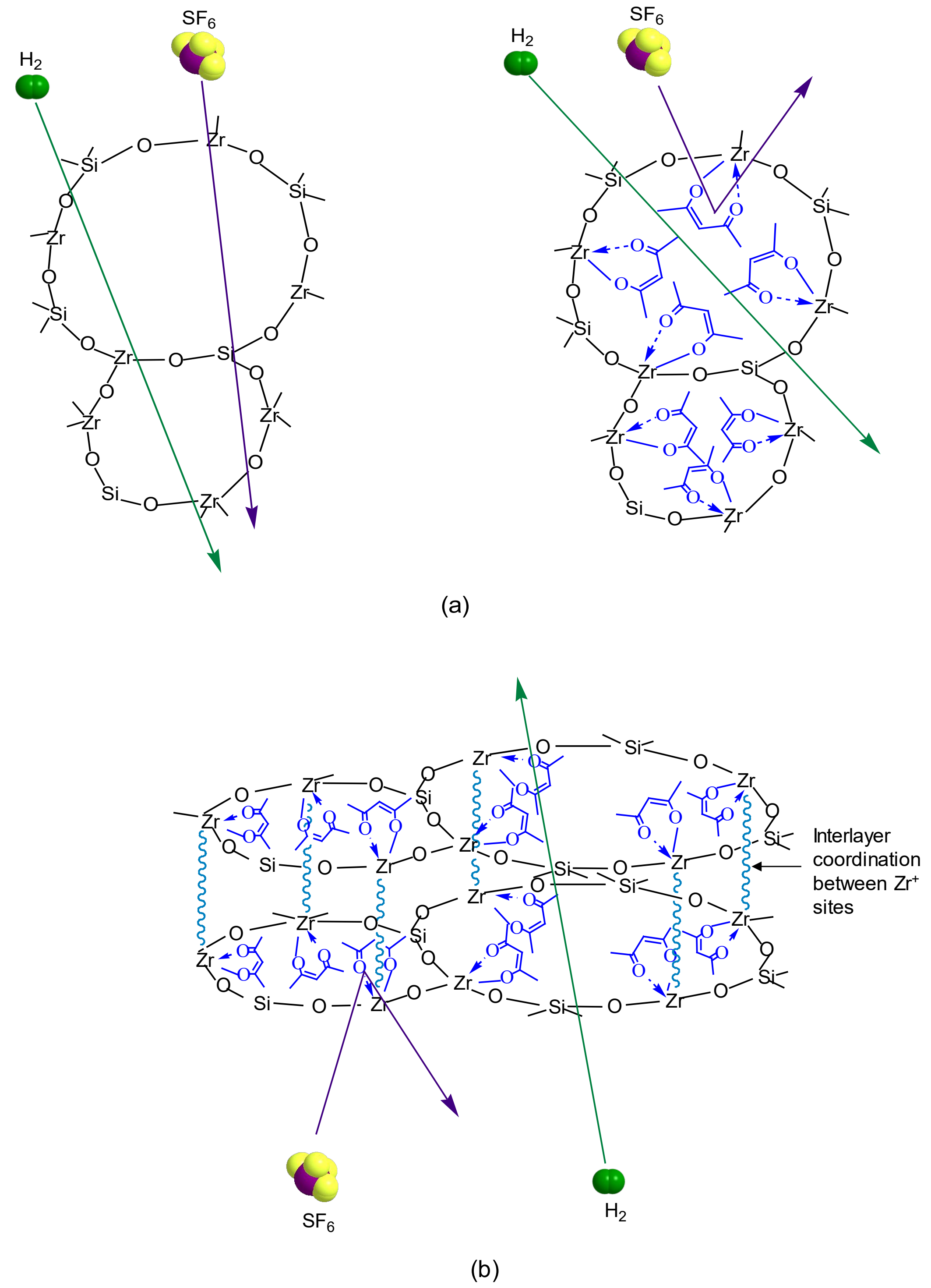

Fig. 8 Schematic image of the intra-particle pore modification effect of acetylacetone chelating ligands forming coordination complexes with Zr atoms and the influence on gas permeation ability; (a) network pore modification theory; (b) interlayer coordination theory.

3.3 Heat-treatment effect on pore size and gas permeation properties of SiO_2-ZrO_2-acac$_2$ membranes

The thermogravimetric results indicate different sections on the TG profile as discussed in section 3.1.2. Therefore, it was interesting to evaluate the gas permeation properties of SZa$_2$-derived membranes fired at different temperatures and the effect that firing temperature exerted on the membrane pore sizes. Fig. 9 shows the molecular size dependence of single-gas permeance at 200 °C (a) and the dimensionless permeance based on He (b) for SZa$_2$-derived membranes heat-treated at temperatures ranging from 250-550 °C under a N_2 flow, as mentioned in section 2.3. Fig. 10 shows the values for single-gas permeance and permeance ratios at 200 °C as a function of heat-treatment temperatures. Gas permeation properties changed as membranes were heat-treated at higher temperatures. A membrane fired at 250 °C showed a low H_2 permeance of 1.8×10^{-7} mol m^{-2} s^{-1} Pa^{-1}, but its H_2/CH_4 selectivity of 50 was higher than with heat-treatment ranging from 300-550 °C. It should be noted that the permeance for large gases such as CF_4 and SF_6 was below the detection levels of 10^{-11} mol m^{-2} s^{-1} Pa^{-1}, and the H_2/SF_6 permeance ratio was assumed to be within the acceptable range of 10^4-10^5, which suggests that these membranes had very dense structures.

After heat-treatment at 300 °C, developments such as a drastic increase in gas permeance and a decrease in gas selectivity were observed (H_2 permeance: ~10^{-6} mol m^{-2} s^{-1} Pa^{-1}, H_2/SF_6 permeance ratio: ~8,000). At 300 °C and above, the changes to gas permeance and permeance ratios were more subdued. It should be noted that H_2 selectivity over large gases such as CF_4 and SF_6 remained above the Knudsen-based values until the membranes were heat-treated at 400 °C. However, a membrane heat-treated at 550 °C showed gas permeance on the order of values like that of the intermediate layer, and H_2 selectivity over large gases such as CF_4 and SF_6 approached Knudsen ratios.

The change in dimensionless permeance with increases in the firing temperature became more pronounced as molecular size increased from H_2 to SF_6. This could have resulted from heat-treatment at higher temperatures causing the acac$^-$ ligands to decompose within the modified pores, which would make the pores larger, which is consistent with thermogravimetric results. The increased pore size increases the access to large gases. High-temperature heat-treatment of SZa$_2$-derived membranes fired at 250 °C, therefore, increases the pore size due to the decomposition of acac$^-$ ligand groups. This decomposition of organics behavior as heat-treatment temperature increases is consistent with the templating effect summarized in Fig. 11. The chelating ligands attached to the Zr$^+$ sites occupied the network pores in the CH$_3$-CH-CH$_2$-CH-CH$_3$ section of the acac$^-$ ligand. As heat-treatment temperature increased, these organic sections began to decompose opening the pores for gas passage, which increased the gas permeance but reduced gas selectivity as larger gases were able to access the network pores. The occupation of network pores can be assumed to be both intraparticle and interparticle. Intraparticle pores exist within individual particles created by spaces between the atomic networks while interparticle pores are the spaces that exist between particles. The interparticle pore-containing ligands decomposed before the intraparticle pore-containing versions, which was inferred by the fact that the membranes continued to show gas selectivity higher than Knudsen ratios even after heat-treatment at 550 °C. This could have been because the intraparticle pore-containing ligands are relatively shielded from heat by the surrounding Si-O-Zr network, much like the encapsulation of carbon in nickel nanoparticles [42].

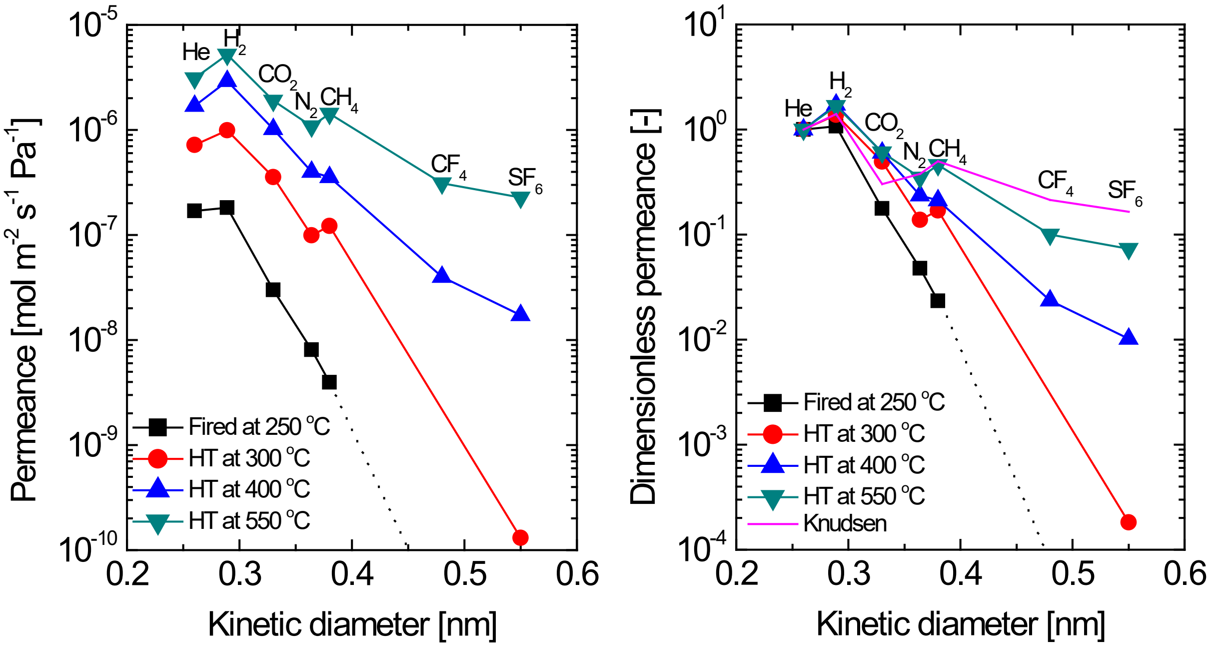

(a)

(b)

Fig. 9 Comparison of the kinetic diameter dependence of single-gas permeance (a) and dimensionless permeance based on He (b) at 200 ºC for SiO_2-ZrO_2-acac$_2$ membranes fired at 250 ºC and heat-treated at different temperatures (300-550 ºC).

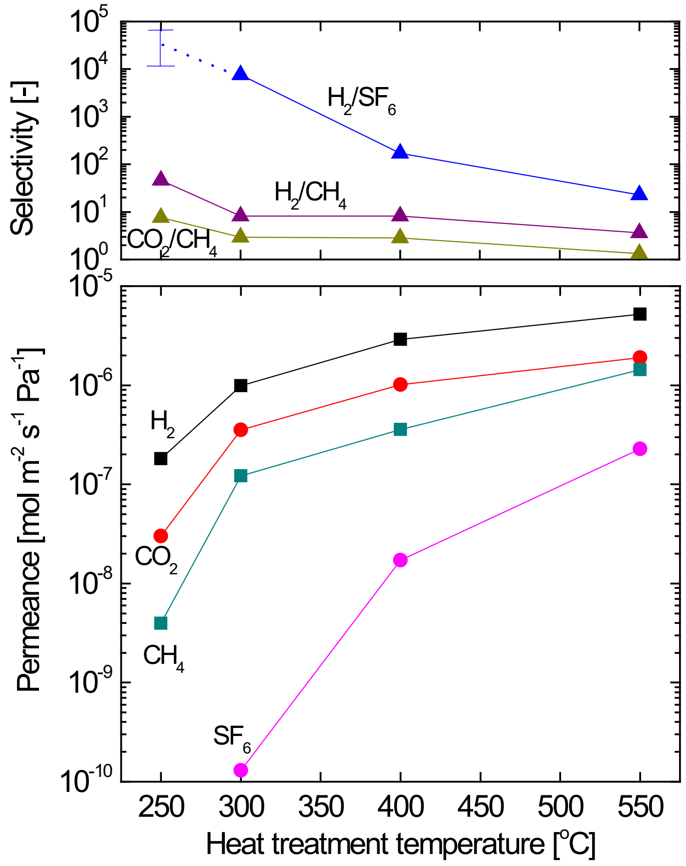

Fig. 10 Heat-treatment temperature (300-550 ºC) dependence of gas permeance and selectivity (H_2/CH_4, H_2/SF_6, CO_2/CH_4) at 200 ºC for SiO_2-ZrO_2-acac$_2$ membranes fired at 250 ºC under a N_2 atmosphere.

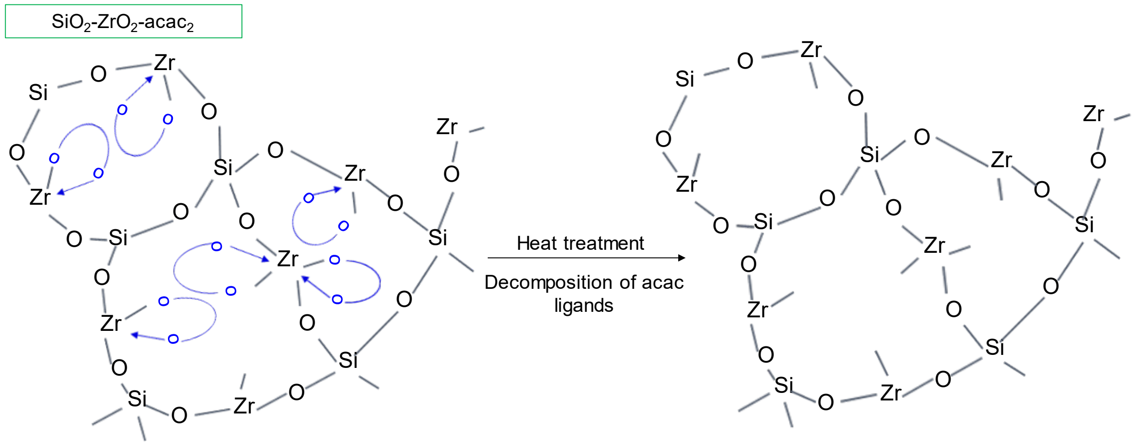

Fig. 11 Schematic diagram of the effect of heat-treatment on the pore size and gas permeation ability of a typical SiO_2-ZrO_2-acac$_2$ membrane.

Fig. 12 shows the single-gas permeance and permeance ratios as functions of temperatures between 50 and 200 ºC for SZa$_2$-derived membranes fired at 250 ºC (a) (He, H_2, CO_2, N_2, CH_4) and heat-treated at 300 ºC (He, H_2, CO_2, N_2, CH_4, SF_6) and 550 ºC (b) (He, H_2, CO_2, N_2, CH_4, CF_4, SF_6). The temperature dependence of permeance and the activation energies of gases were fitted and calculated using the modified gas translation model (Eq. 1). The model showed a very good fit with the experimental data and should be regarded as a viable representation of gas-membrane behavior.

$$P_i = \frac{k_{o,i}}{\sqrt{M_i RT}} exp\left(-\frac{E_{p,i}}{RT}\right) \qquad (1)$$

For membranes fired at 250 ºC, the permeance of all gases (He, H_2, N_2, CH_4) increased with increases in temperature, suggesting an activated diffusion mechanism. The exception to this was CO_2, which showed an increase in permeance as the temperature decreased, which suggests a surface-diffusion mechanism. Gas selectivities (H_2/CH_4, CO_2/CH_4, CO_2/N_2) increased as temperature decreased. In particular, for gas permeance measured at 50 ºC, H_2/CH_4 and CO_2/CH_4 selectivities reached 100 and 60, respectively.

Membranes heat-treated at 300 ºC showed the same trend as the original membrane fired at 250 ºC with gas permeance (He, H_2, N_2, CH_4) increasing as the temperature increased with the noted exception of CO_2 that exhibited a surface-diffusion mechanism. However, the slopes of the temperature dependence of gas permeance followed different trends, and membranes fired at 250 ºC showed increases in the slope as the molecular size increased, but the slope decreased with molecular size for membranes heat-treated at 300 ºC.

When heat-treated to 550 ºC, the permeance of gases (N_2, CF_4, SF_6) decreased as temperature increased except for small gases (He, H_2 and CH_4) that continued to show smaller activation energies (He: 5.7, H_2: 5.1, CH_4: 5.1 kJ mol^{-1}) compared with 250 ºC-fired membranes (He: 12, H_2: 13, CH_4: 20 kJ mol^{-1}). The transition in membrane permeation characteristics can be clearly observed in the gas selectivity plot. As a membrane is heat-treated to 300 ºC, there is a drastic decrease in gas selectivity (H_2/CH_4, CO_2/CH_4, CO_2/N_2), which is reduced even further for membranes heat-treated at 550 ºC with no considerable variation in permeation temperature. Based on these results, it can be concluded that the pore morphology in a 250 ºC-fired membrane is such that gas separation with high selectivity can be expected by altering the operating temperature, whereas membranes heat-treated to 550 ºC can accomplish no gas separation at different operating temperatures since the pores are not selective for gases.

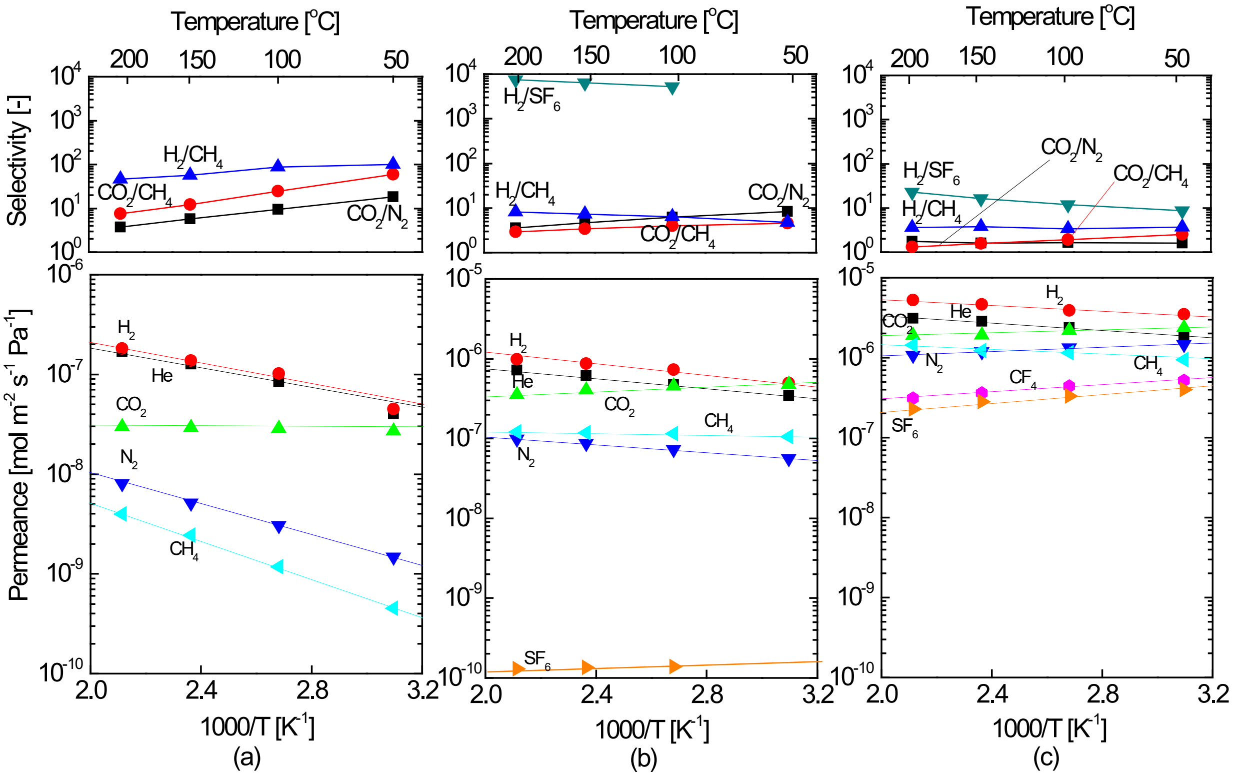

Fig. 12 Temperature dependence of gas permeance at temperatures ranging from 50-200 ºC for SiO_2-ZrO_2-acac$_2$ membranes fired at 250 ºC (a) and heat-treated at 300 ºC (b) and 550 ºC (c) under N_2.

Fig. 13 shows the relationship between the activation energies of gases (He, H_2, N_2, CH_4, SF_6) and the kinetic diameter for SZa$_2$-derived heat-treatment ranging from 250-550 ºC, for isoeugenol-modified TiO_2-ZrO_2-derived [39] and polyimide membranes [52, 53]. For SZa$_2$-derived membranes heat-treated at 250 ºC, isoeugenol-modified, TiO_2-ZrO_2-derived, and polyimide membranes, the activation energy increases as the kinetic diameter increases, as indicated in Fig. 13 via the data points in the solid-line circle. These results indicate a similar gas permeation mechanism in these membranes, although the polymer membrane showed higher activation energies across all gases. This behavior (increased activation energy of gas permeance with kinetic diameter of gases) is a solution-diffusion mechanism that is accepted as the transport mechanism in polymer membranes [54, 55]. As for the polyimide membranes studied by Villaluenga *et al.* [52] and Hirayama *et al.* [56], the interaction between the polymer and each gas (He, H_2, N_2, CH_4) corresponding to the heat of sorption, ΔH_s, is very small so that the high activation energies of permeation observed should be attributed to diffusivity rather than to solubility, even if the solubility coefficient is thermodynamic in nature. The thermodynamic nature of gas diffusivity in polymer membranes can be explained by the fact that polymer chains corresponding to voids vibrate relative to temperature so that activation energy increases with kinetic diameter. Thus, based on the observed trend, this phenomenon could also be attributed to SZa_2-derived membranes fired at 250 °C.

In contrast, as indicated by data points in the dashed-line circle in Fig. 13, the kinetic diameter dependence of the apparent activation energy of SZa_2-derived membranes heat-treated at 300-550 °C showed a trend whereby activation energy decreased with kinetic diameter. This was apparent because heat-treatment at higher temperatures decomposed the organic content in the modified network structure, which resulted in enlarged network pores that allowed easier access to larger gases for these membranes. Fig. S5 also compares the heat-treatment temperature dependence of the apparent activation energies of He and N_2, which clearly displays a sharper reduction in the activation energy of N_2 than that of He and suggests the creation of larger pores. However, small gases (He and H_2) showed higher activation energies indicating the presence of pores with sizes in the range of the kinetic diameters of He and H_2 even after firing at higher temperatures. These two observations are evidence of a bimodal pore structure. Therefore, the heat-treatment of membranes affects the pore structure enough to affect the permeation properties of the membrane.

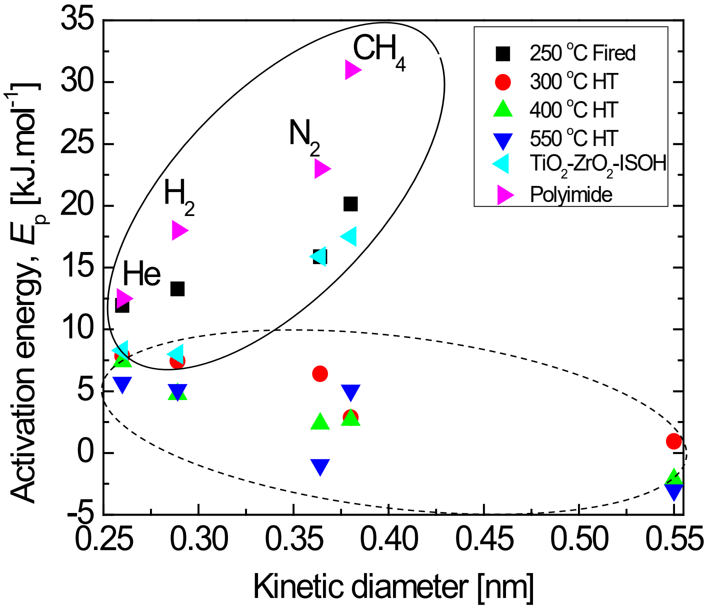

Fig. 13 Kinetic diameter dependence of gas activation energies (He, H_2, N_2, CH_4, SF_6) for SiO_2-ZrO_2-acac$_2$ membranes fired at 250 °C and heat-treated at 300, 400 or 550 °C under N_2 compares with that of isoeugenol (ISOH)-modified TiO_2-ZrO_2 [39] and polyimide [52, 53] membranes.

Fig. 14 shows the trade-off plot for the H_2/SF_6 permeance ratio as a function of H_2 permeance for two different membranes fired at 250 °C and heat-treated at 300, 400 or 550 °C. It should be noted that the SF_6 permeance for a membrane fired at 250 °C was assumed to be on the order of 10^{-11}, which is below the detection limit, and, therefore, the H_2/SF_6 permeance ratio was assumed to be within a reasonable limit of 10^4 to 10^5. It was apparent that all H_2/SF_6 permeance ratios were above the Knudsen ratio irrespective of heat-treatment temperature. The solid line in Fig. 14 is the trade-off line that can be drawn to align with the trade-off points. A membrane with high H_2/SF_6 selectivity generally shows a low H_2 permeance, and vice versa. A similar trend was observed for H_2/N_2 and H_2/CH_4 as functions of H_2 permeance (Fig. S6 (a) and (b)). When the trade-off line is considered, membranes heat-treated at 300 °C provided a favorable trade-off point by maintaining a good balance between H_2/SF_6 (1,800-7600) selectivity and H_2 permeance (0.4-1 x 10^{-6} mol m^{-2} s^{-1} Pa^{-1}). Although membranes fired at 250 °C exhibited a higher H_2/SF_6 selectivity (>

18,000), that for a membrane heat-treated at 300 °C was not far below, but with almost 10 times the order of H_2 permeance (1.8×10^{-7} mol m^{-2} s^{-1} Pa^{-1}). Thus, a membrane heat-treated at 300 °C delivers a better trade-off than other membranes with high H_2 permeance and H_2/SF_6 selectivity.

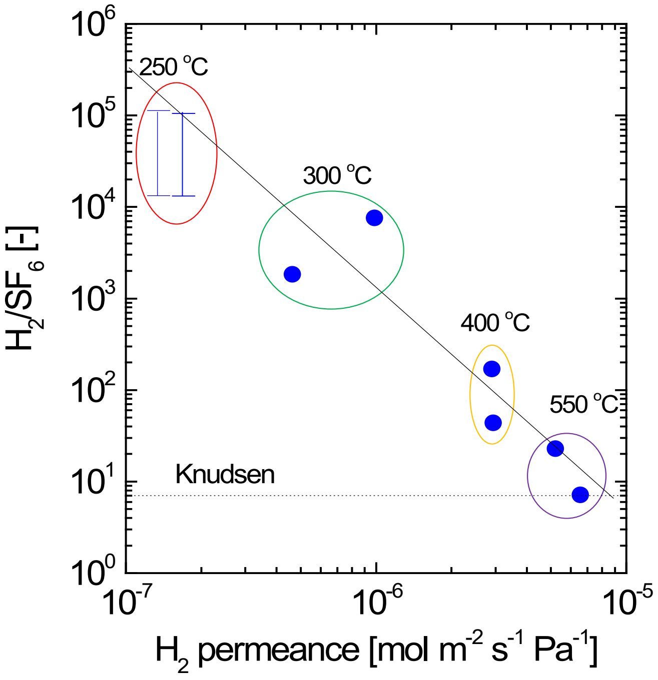

Fig. 14 H_2/SF_6 permeance ratio as a function of H_2 permeance at 200 °C for membranes fired at 250 °C and heat-treated at 300, 400 or 550 °C.

4. Conclusions

A chemical modification of SiO_2-ZrO_2 via the sol-gel method was successfully accomplished by chelating acetylacetonate (acac$^-$) with zirconium tetrabutoxide (ZrTB) prior to co-hydrolysis and condensation with tetraethoxysilane (TEOS), which was then used to fabricate a gas separation layer by coating the acac$^-$-modified SiO_2-ZrO_2 sol onto a SiO_2-ZrO_2 intermediate layer. Acac$^-$-modified SiO_2-ZrO_2-derived membranes were then fabricated by firing under N_2 at 250 °C followed by heat-treatments that ranged from 300-

550 °C under N_2. Single-gas permeation experiments were carried out to examine the effect of chelating agents on the resultant modification of the pores, which affected the gas permeation properties of the membrane.

The acac$^-$-modified SiO_2-ZrO_2-derived membrane showed H_2 permeance of 9.9 x 10 $^{-7}$ with a H_2/SF_6 permeance ratio of 7,600, which was better than the results when using a pure SiO_2-ZrO_2-derived membrane (H_2 permeance: 1.4 x 10 $^{-6}$ mol m^{-2} s^{-1} Pa^{-1}, H_2/SF_6 permeance ratio: 11). When an acac$^-$-modified SiO_2-ZrO_2-derived membrane prepared at 250 °C (H_2 permeance: 1.8 x 10^{-7} mol m^{-2} s^{-1} Pa^{-1}, H_2/CH_4: 100, CO_2/CH_4: 60 at 50 °C) was heat-treated at 550 °C, the result was improved H_2 permeance of 5.2 x 10^{-6} mol m^{-2} s^{-1} Pa^{-1} with low permeance ratios (H_2/CH_4: 3, H_2/SF_6: 9) at 50 °C. The 250 °C-fired acac$^-$-modified SiO_2-ZrO_2-derived membranes exhibited a gas permeation mechanism similar to polymer membranes, and the 300 °C-heat-treated version showed the best trade-off between H_2 permeance and the H_2/SF_6 permeance ratio.

References

1. N. W. Ockwig, T. M. Nenoff, Membranes for hydrogen separation, Chem. Rev. 107 (2007) 4078-4110.
2. S. Adhikari, S. Fernando, Hydrogen membrane separation techniques, Ind. Eng. Chem. Res. 45 (2006) 875-881.
3. H. Li, Z. Song, X. Zhang, Y. Huang, S. Li, Y. Mao, H. J. Ploehn, Y. Bao, M. Yu, Ultrathin, molecular-sieving graphene oxide membranes for selective hydrogen separation, Science 342 (2013) 95-98.
4. M. Kanezashi, D. Fuchigami, T. Yoshioka, T. Tsuru, Control of Pd dispersion in sol-gel-derived amorphous silica membranes for hydrogen separation at high temperatures, J. Membr. Sci. 439 (2013) 78-86.
5. S-J. Ahn, A. Takagaki, T. Sugawara, R. Kikuchi, S. T. Oyama, Permeation properties of silica-zirconia composite membranes supported on porous alumina substrates, J. Membr. Sci. 526 (2017) 409-416.

6. S.-W. Chuang, S. L.-C. Hsu, Y.-H. Liu, Synthesis and properties of fluorine-containing polybenzimidazole/silica nanocomposite membranes for proton exchange membrane fuel cells, J. Membr. Sci. 305 (2007) 353-363.
7. Y. Zhang, J. Sunarso, S. Liu, R. Wang, Current status and development of membranes for CO_2/CH_4 separation: a review, Int. J. Green Gas Control. 12 (2013) 84-107.
8. M. A. Carreon, S. Li, J. L. Falconer, R. D. Noble, Alumina-supported SAPO-34 membranes for CO_2/CH_4 separation, J. Am. Chem. Soc. 130 (2008) 5412-5413.
9. C. E. Powell, G. G. Qiao, Polymeric CO_2/N_2 gas separation membranes for the capture of carbon dioxide for power plant flue gases, J. Membr. Sci. 279 (2006) 1-49.
10. L. Zhao, E. Riensche, R. Menzer, L. Blum, D. Stolten, A parametric study of CO_2/N_2 gas separation membrane processes for post-combustion capture, J. Membr. Sci. 325 (2008) 284-294.
11. D. C. Nymeijer, T. Visser, R. Assen, M. Wessling, Composite hollow fiber gas-liquid membrane contactors for olefin/paraffin separation, Sep. Purif. Technol. 37 (2004) 209-220.
12. B. N. Nair, K. Keizar, W. J. Elferink, M. J. Gilde, H. Verweij, A. J. Burggraaf, Synthesis, characterization and gas permeation studies on microporous silica and alumina-silica membranes for separation of propane and propylene, J. Membr. Sci. 116 (1996) 161-169.
13. S. Yun, J. H. Ko, S. T. Oyama, Ultrathin palladium membranes prepared by a novel electric field assisted activation, J. Membr. Sci. 369 (2011) 482-489.
14. S. Yun, S. T. Oyama, Correlations in palladium membranes for hydrogen separation: a review, J. Membr. Sci. 375 (2011) 28-45.
15. M. Kanezashi, Sol-Gel Derived Silica Membranes, Encyclopedia of Membrane Science and Technology, John Wiley and Sons, 2013
16. B. Ballinger, J. Motuzas, S. Smart, J. C. Diniz da Costa, Palladium cobalt binary doping of molecular sieving silica membranes, J. Membr. Sci. 451 (2014) 185-191
17. R. M. de Vos, H. Verweij, High-selectivity, high-flux silica membranes for gas separation, Science. 279 (1998) 1710-1711.
18. R. M. de Vos, H. Verweij, Improved performance of silica membranes for gas separation, J. Membr. Sci. 143 (1998) 37-51.

19. A. Peta Dral, J. E. ten Elshof, Organic groups influencing microporosity in organosilicas, Micropor. Mesopor. Mater. 267 (2018) 267-273.
20. M. Kanezashi, Y. Yoneda, H. Nagasawa, T. Tsuru, K. Yamamoto, J. Ohshita, Gas permeation properties for organosilica membranes with different Si/C ratios and evaluation of microporous structures, AIChE J. 63 (2017) 4491-4498.
21. N. K. Raman, C. J. Brinker, Organic “template” approach to molecular sieving silica membranes, J. Membr. Sci. 105 (1995) 273-279.
22. K. Yoshida, Y. Hirano, H. Fujii, T. Tsuru, M. Asaeda, Hydrothermal stability and performance of silica-zirconia for hydrogen separation in hydrothermal conditions, J. Chem. Eng. Jpn 34 (2001) 523-530.
23. D. Uhlmann, S. Liu, B. P. Ladewig, J. C. D. da Costa, Cobalt-doped silica membranes for gas separation, J. Membr. Sci. 326 (2009) 316-321.
24. Y. Gu, P. Hacarlioglu, S. T. Oyama, Hydrothermally stable silica-alumina composite membranes for hydrogen separation, J. Membr. Sci. 310 (2008) 28-37.
25. V. Tajer-Kajinebaf, H. Sarpoolaky, T. Mohammadi, Sol-gel synthesis of nanostructured titania-silica mesoporous membranes with photo-degradation and physical separation capacities for water purification, Ceram. Int. 40 (2014) 1747-1757.
26. Y. Gu, S T. Oyama, Permeation properties and hydrothermal stability of silica-titania membranes supported on porous alumina substrates, J. Membr. Sci. 345 (2009) 267-275.
27. M. Asaeda, Y. Sakou, J. Yang, K. Shimasaki, Stability and performance of porous silica-zirconia composite membranes for pervaporation of aqueous organic solutions, J. Membr. Sci. 209 (2002) 163-175.
28. W. Puthai, M. Kanezashi, H. Nagasawa, K. Wakamura, H. Ohnishi, T. Tsuru, Effect of firing temperature on water permeability of SiO_2-ZrO_2 membranes for nanofiltration, J. Membr. Sci. 497 (2016) 348-356.
29. P. Pandey, R. S. Chauhan, Membranes for gas separation, Prog. Polym. Sci. 26 (2001) 853-893.
30. L. Li, H. Qi, Gas separation using sol-gel derived microporous zirconia membranes with high hydrothermal stability, Ch. J. Chem. Eng. 23 (2015) 1300-1306.

31. C. A. Milea, C. Bogatu, A. Duta, The influence of parameters in silica sol-gel process, in: Bulletin of the Transilvania University of Brasov, Series I: Engineering sciences Vol. 4 (53), 2011, pp. 59-66.
32. D. A. Ward, E. I. Ko, Preparing catalytic materials by the sol-gel method, Ind. Eng. Chem. Res. 34 (1995) 421-433.
33. N. Stock, S. Biswas, Synthesis of metal-organic frameworks (MOFs): routes to various MOF topologies, morphologies, and composites, Chem. Rev. 112 (2012) 933-969.
34. S. Basu, A. Cano-Odena, I. F. J. Vankelecom, MOF-containing mixed-matrix membranes for CO_2/CH_4 and CO_2/N_2 binary gas mixture separations, Sep. Purif. Technol. 81 (2011) 31-40.
35. O. G. Nik, X. Y. Chen, S. Kaliaguine, Functionalized metal organic framework-polyimide mixed matrix membranes for CO_2/CH_4 separation, J. Membr. Sci. 413-414 (2012) 48-61.
36. D. Hoebbel, T. Reinert, H. Schmidt, E. Arpac, On the hydrolytic stability of organic ligands in Al-, Ti- and Zr-alkoxide complexes, J. Sol-Gel Sci. Technol. 10 (1997) 115-126.
37. C. Janiak, Engineering coordination polymers towards applications, Dalton Trans. (2003) 2781-2804.
38. D. Peter, T. S. Ertel, H. Bertagnolli, EXAFS study of zirconium alkoxides as precursors in sol-gel process: II. The influence of the chemical modification, J. Sol-Gel Sci. Technol. 5 (1995) 5-14.
39. T. Fukumoto, T. Yoshioka, H. Nagasawa, M. Kanezashi, T. Tsuru, Development and gas permeation properties of microporous amorphous TiO_2-ZrO_2-organic composite membranes using chelating ligands, J. Membr. Sci. 461 (2014) 96-105.
40. G. I. Spijksma, C. Huiskes, N. E. Benes, H. Kruidhof, D. H. A. Blank, V. G. Kessler, H. J. M. Bouwmeester, Microporous zirconia-titania composite membranes derived from diethanolamine-modified precursors, Adv. Mater. 18 (2006) 2165-2168.
41. T. Tsuru, Nano/subnano-tuning of porous ceramic membranes for molecular separations, J. Sol-Gel Sci. Technol. 46 (2008) 349-361.
42. M. Chen, L. Bin, S. Huai-he, Z. Lin-jie, Preparation of carbon encapsulated metal magnetic nanoparticles by an instant pyrolysis method, New Carbon Mater. 25 (3) (2010) 199-204.

43. Y. Li, S. Chen, H. Hu, C. Zou, Z. Chen, X. Ma, A meltable precursor for zirconium carbide ceramics and C/C-ZrC composites, Ceram. Int. 44 (2018) 10175-10180
44. R. W. Silverstein, G. C. Bassler, Spectrometric identification of organic compounds, J. Chem. Ed. 39 (1962) 546-553.
45. A. L. Smith, Infrared spectra-structure correlations for organosilicon compounds, Spectrochimica Acta. 16 (1960) 87-105.
46. J. Coates, Interpretation of infrared spectra, a practical approach, Encyclopedia of Analytical Chemistry, doi: 10. 1002/9780470027318. A5606
47. Z.-G. Wu, Y.-X. Zhao, D.-S. Liu, The synthesis and characterization of mesoporous silica-zirconia aerogels, Micropor. Mesopor. Mater. 68 (2004) 127-132.
48. T. Niimi, H. Nagasawa, M. Kanezashi, T. Yoshioka, K. Ito, T. Tsuru, Preparation of BTESE-derived organosilica membranes for catalytic membrane reactors of methylcyclohexane dehydrogenation, J. Membr. Sci. 455 (2014) 375-383.
49. J. Yang, D. Gong, G. Li, G. Zeng, Q. Wang, Y. Zhang, G. Liu, P. Wu, E. Vovk, Z. Peng, X. Zhou, Y. Yang, Z. Liu, Y. Sun, Self-assembly of thiourea-crosslinked graphene oxide framework membranes toward separation of small molecules, Adv. Mater. 30 (2018) 1705775 (1-8)
50. T. Ikeda, Y. Akiyama, Y. Oumi, A. Kawai, F. Mizukami, The topotactic conversion of a novel layered silicate into a new framework zeolite, Angew. Chem. Int. Ed. 43 (2004) 4892-4896.
51. T. Uragami, K. Okazaki, H. Matsugi, T. Miyata, Structure and permeation characteristics of an aqueous ethanol solution of organic-inorganic hybrid membranes composed of poly(vinyl alcohol) and tetraethoxysilane, Macromolecules 35 (2002) 9156-9163.
52. J. P. G. Villaluenga, B. Seoane, J. Hradil, P. Sysel, Gas permeation characteristics of heterogeneous ODPA-BIS P polyimide membranes at different temperatures, J. Membr. Sci. 305 (2007) 160-168.
53. K. Haraya, K. Obata, N. Itoh, Y. Shindo, T. Hakuta, Y. Yoshitome, Gas permeation and separation by an asymmetric polyimide hollow fiber membrane, J. Membr. Sci. 41 (1989) 23-35.

54. S. A. Stern, S. R. Sampat, S. S. Kulkarni, Test of a “free-volume” model of gas permeation through polymer membranes. II. Pure Ar, SF_6, CF_4, and $C_2H_2F_2$ in polyethylene, J. Polym. Sci., Part B: Polym. Phys. 24 (1986) 2149-2166.
55. J. P. G. Villaluenga, B. Soane, Experimental estimation of gas-transport properties of linear low-density polyethylene membranes by an integral permeation method, J. Appl. Polym. Sci. 82 (2001) 3013-3021.
56. Y. Hirayama, T. Yoshinaga, K. Kusuki, K. Ninomiya, T. Sakakibara, T. Tamari, Relation of gas permeability with structure of aromatic polyimides I, J. Membr. Sci. 111 (1996) 169-182.